Natland, J.H., Storms, M.A., et al., 1993
Proceedings of the Ocean Drilling Program, Scientific Results, Vol. 132

3. MAGNETIC PROPERTIES OF PLIOCENE-PLEISTOCENE SEDIMENTS FROM HOLE 810C, SHATSKY RISE, AND IMPLICATIONS FOR THE ORIGIN AND CORRELATABILITY OF THEIR MAGNETIC SUSCEPTIBILITY VARIATIONS[1]

Evelyn L. Polgreen,[2] William W. Sager,[2] Frank R. Rack,[2,3] and Robert J. van Waasbergen[4]

ABSTRACT

Shatsky Rise, located in the northwestern Pacific, is covered with a thick cap of pelagic, carbonate-dominated sediments with a secondary eolian component. Ocean Drilling Program Leg 132 drilled Pleistocene to Maastrictian oozes at Site 810, near the summit of the Shatsky Rise, using the advanced hydraulic piston corer to achieve virtually complete recovery in the upper 127 m below the seafloor. The down-core stratigraphy of whole-core magnetic susceptibility displays peaks with amplitudes of 30–40 $\times 10^{-8}$ SI and widths of tens of centimeters. Overall, magnetic susceptibility values are predominantly negatively correlated with calcium carbonate percentages. Similar variations in other deep-sea sediments have been interpreted as records of glacial-interglacial climate cycles.

A study of the magnetic properties of Pliocene-Pleistocene sediments was undertaken to understand the nature of the magnetic susceptibility cycles. The acquisition and demagnetization properties of natural and artificial magnetic remanences were examined. Isothermal remanences approach saturation at 30 to 40 mT, although a small amount of magnetization is acquired in higher fields. This observation implies that the primary magnetic mineral is titanomagnetite, but there is also a secondary, higher coercivity component, perhaps hematite or goethite. Ratios of saturation isothermal remanent magnetization to magnetic susceptibility and saturation isothermal remanence vs. anhysteretic remanent magnetization suggest that the magnetic susceptibility peaks result mainly from high relative variations in magnetite concentration. Moreover, consistent ratios of saturation isothermal remanent magnetization to magnetic susceptibility imply that the size of the magnetic particles is relatively uniform.

Scanning electron microscopy and energy-dispersive X-ray analyses show titanomagnetite with dissolution features in some of the grains. Energy-dispersive X-ray analysis of a few samples suggests two size fractions with different titanium concentrations. These two size ranges are present in high, medium, and low susceptibility samples. These observations suggest magnetic grains transported from two source regions or differential reduction diagenesis of the titanomagnetite grains.

Magnetic susceptibility peaks from Hole 810C were correlated with those from Deep Sea Drilling Project Site 577, 11 km to the west and 50 m deeper. Peaks in one or the other of the two holes are commonly missing or cannot be correlated. In all, only 35% of the peaks in Hole 810C match those in Hole 577. These observations suggest that sedimentation atop Shatsky Rise has been disturbed by local erosion. Missing features in Hole 577 suggest a greater degree of erosion and perhaps stronger currents at that site. As a consequence of possible erosion at both sites, it may be difficult to obtain continuous sediment sections with adequate time control for paleoclimate studies in this locality.

INTRODUCTION

Ocean Drilling Program (ODP) Leg 132 drilled Site 810 near the summit of Shatsky Rise, 1800 km east of Japan in the northwestern Pacific (Fig. 1). Hole 810C lies at a water depth of 2623 m, well above the carbonate compensation depth (CCD), which results in the preservation of carbonate sediments. Hole 810C penetrated 143.81 m of mainly nannofossil ooze, ranging in age from Pleistocene to early Maastrichtian with several hiatuses in the upper Miocene to lower Eocene, lower Eocene to upper/lower Paleocene, and lower Paleocene to upper Maastrichtian sections (Premoli Silva et al., this volume; Sager et al., this volume). High-resolution magnetic susceptibility measurements of whole-core sections from Hole 810C, taken aboard ship, displayed peaks with amplitudes of 30–40 $\times 10^{-8}$ SI and widths of tens of centimeters. These data show a negative correlation to calcium carbonate percentages (Rack et al., this volume). Similar variations in deep-sea sediments elsewhere have been interpreted as records of glacial-interglacial climate cycles (e.g., Kent, 1982; Mead et al., 1986; Robinson, 1986; Bloemendal et al., 1988).

Magnetic susceptibility measurements have been used as indicators of changing sedimentary parameters. Variations in grain size, mineralogy, and concentration of magnetic grains reflect pre- and post-depositional environmental changes, yielding clues to fluctuations in climate and depositional environment. For example, magnetic susceptibility records of the loess in China have been examined for clues to their relationship to climate-forcing orbital frequencies (e.g., Kukla et al., 1988; Kukla and An, 1989). Magnetic susceptibility has also been compared to commonly used proxy paleoclimate indicators, such as calcium carbonate percentages and oxygen isotopes in deep-sea sediments (e.g., Kent, 1982; Mead et al., 1986; Robinson, 1986; Bloemendal et al., 1988; Bloemendal and deMenocal, 1989). Recent trends in magnetic susceptibility paleoclimate studies are to attempt correlation of susceptibility records over ocean basins (Bloemendal et al., 1992) and to link continental and marine sediment sections by comparing magnetic susceptibility and oxygen isotope records—for example, correlating the loess sequences in China with age-equivalent sections in the Western Pacific (Kukla et al., 1988; Hovan et al., 1989; Maher and Thompson, 1992).

Magnetic susceptibility records from Hole 810C provide new data, which could be correlated with other sedimentary records in the northwestern Pacific. The position of the site, downwind from the Asian continent, makes it ideal for the study of eolian flux to marine sediments in the North Pacific, and therefore it is a potential link between land-to-sea magnetic susceptibility records. The Pliocene-Pleistocene record is particularly important because of an apparent increase in the dust flux from continents to the North Pacific during this time period (Rea and Leinen, 1988).

[1] Natland, J.H., Storms, M.A., et al., 1993. *Proc. ODP, Sci. Results,* 132: College Station, TX (Ocean Drilling Program).

[2] Department of Oceanography, Texas A&M University, College Station, TX 77843-3146, U.S.A.

[3] Ocean Drilling Program, 1000 Discovery Drive, Texas A&M University, College Station, TX 77845-9547, U.S.A.

[4] Scripps Institution of Oceanography, University of California, San Diego, La Jolla, CA 92093-0215, U.S.A.

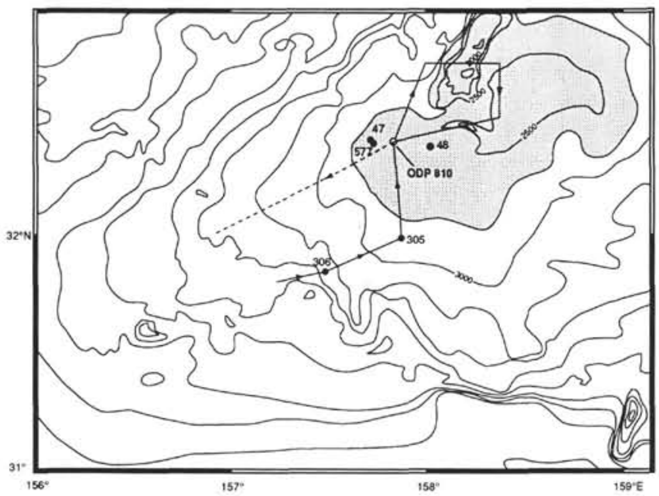

Figure 1. Location map, showing ODP Site 810 near the summit of Shatsky Rise, together with several Deep Sea Drilling Project sites. Bathymetric contours shown in meters.

In this study, we sought to understand the source of the magnetic susceptibility variations by characterizing rock magnetic properties. This step is necessary to make a convincing case for regional and global correlation of this signal. We also compared the magnetic susceptibility records from ODP Hole 810C with susceptibility measurements of the cores from nearby Deep Sea Drilling Project (DSDP) Hole 577. We reasoned that their records should be similar, given the small distance (11 km) between the sites. We hoped that the comparison of the two records might give clues about the sedimentation atop topographic highs such as the Shatsky Rise and the suitability of these records for use in regional correlations.

METHODS

Volume magnetic susceptibility was measured at a spacing of 5 cm aboard *JOIDES Resolution* on whole-round core sections from Hole 810C (0–80 mbsf), using a Bartington Instruments MS-2 susceptibility meter. This instrument has an 80-mm sensing loop and uses an inducing field of 0.1 mT RMS at a frequency of 470 Hz. The meter is capable of measuring volume susceptibility differences as small as 10^{-8} SI.

Archive halves of sections from Hole 577 were measured at Scripps Institution of Oceanography, using a similar pass-through system with an 80-mm sensing loop at 2-cm intervals. Because of the sensing-window width of the loop sensor, this close spacing has the effect of smoothing the data slightly. These records were visually correlated with those from Hole 810C, using magnetic age boundaries as tie points (Bleil, 1985; Sager et al., this volume). Peaks were correlated between the two holes, using their shapes and magnitudes as the basis for comparison. Ages for specific depths in both holes were derived from magnetic polarity stratigraphies (Bleil, 1985; Sager et al., this volume), which in turn rely upon the widely used polarity time scale of Berggren et al. (1985). Although recent revisions (e.g., Cande and Kent, 1992) have changed the ages of boundaries, the changes do not affect the conclusions reached in this study.

Sections from Cores 132-810C-2H and -3H, near the Brunhes/Matuyama polarity boundary (Sager et al., this volume), were chosen for detailed study of the relationship between their magnetic properties and the smaller scale changes in magnetic susceptibility. This upper part of the record from Hole 810C contains features that match excursions in the record from Hole 577 and hence may be the best part of the core for use in time series analyses, taking into account the poor correlation in the majority of the records from the two sites. One hundred twenty-one samples were taken from the working halves of these cores at intervals of approximately 10 cm, using 6-cm^3 plastic cubes. The susceptibility of each discrete sample was measured with a Bartington MS-2 meter similar to the one used on the ship, but with a 36-mm dual-frequency loop designed for discrete samples.

Magnetic remanence was measured using a CTF cryogenic magnetometer in the Geophysics Department of Texas A&M University. In addition to measuring the natural remanent magnetization (NRM), samples were demagnetized stepwise using an alternating magnetic field (AF). Twenty pilot samples were demagnetized in fields of up to 100 mT. The remaining samples were demagnetized in fields of up to 50 mT, past their mean destructive field (MDF).

Two artificial remanences were imparted to the 20 pilot samples—an anhysteretic remanent magnetization (ARM) and a saturation isothermal remanent magnetization (SIRM). The ARM was given to each sample by exposing it to a constant 0.05-mT field and a slowly decaying 100-mT alternating field. After measuring the ARM, each sample was AF demagnetized in fields up to 100 mT. The IRM was imparted using an impulse magnetizer in which capacitors release a surge of current through a coil to produce a field of up to 1200 mT for about 2 ms. Using this device, pilot samples were magnetized in progressively higher fields until saturation occurred. These saturated samples were then AF demagnetized stepwise in fields to 100 mT.

After the IRM was AF demagnetized, the pilot samples were reversed and given an IRM in the opposite direction. This back field was applied to each sample until its IRM intensity dropped to zero, allowing remanence coercivities to be determined for these samples.

All magnetic-property data can be obtained from the Ocean Drilling Program database.

Magnetic separates were taken from pilot Samples 132-810C-2H-3, 86–88 cm (5.6×10^{-5} SI), -2H-4, 45–47 cm (2.4×10^{-5} SI), and -3H-5, 6–8 cm (10.3×10^{-5} SI). These three were chosen to represent medium-, low-, and high-susceptibility samples, respectively. The separates were examined using a scanning electron microscope (SEM) and energy-dispersive X-ray analysis (EDX). Separates were obtained in two ways. For both methods, each sample was dispersed ultrasonically in de-ionized water. The water containing the dispersed sample was poured into a magnetic separator. The separator carried the sample, suspended in water, past a strong magnet held in a Lexan sleeve. The sleeve, still holding the magnet, was then removed from the system. The sample was obtained by removing the magnet and rinsing the sleeve into a sample holder using additional de-ionized water. This method probably obtained a large to intermediate size fraction: the coarsest particles were too heavy to be suspended, and the finest particles could have been swept from the sleeve by the flowing water. A coarse fraction was obtained by stirring the water-sediment mixture and placing the magnet/sleeve in the bottom of the beaker. A finer fraction was captured by allowing the sleeve and magnet to stand in the beaker overnight, so that suspended magnetic material could settle on the sides of the sleeve.

RESULTS

Susceptibility Variations and Trends

Both whole-core and discrete susceptibility measurements show two levels of variation: larger scale trends that vary over spans of tens of meters and smaller wavelength fluctuations of 1 m or less.

In the whole-core measurements (Fig. 2), the general downhole trend of magnetic susceptibility values is a rise from 1.35×10^{-5} SI to 5.39×10^{-5} SI in the first 1.5 m below the seafloor (mbsf) with a rapid drop to 0.76×10^{-5} SI before 2 mbsf. Between 2 and 5 mbsf, values range from 8.34×10^{-5} SI to 0.32×10^{-5} SI. A broad systematic decrease of about 5×10^{-5} SI begins at approximately 15 mbsf for lower Pleistocene sediments and levels out at about 30 mbsf for upper Pliocene sediments. From 80 to 95 mbsf, an overall increase of approximately the same magnitude takes place in the upper to middle Miocene section. In between, susceptibility values show broad oscil-

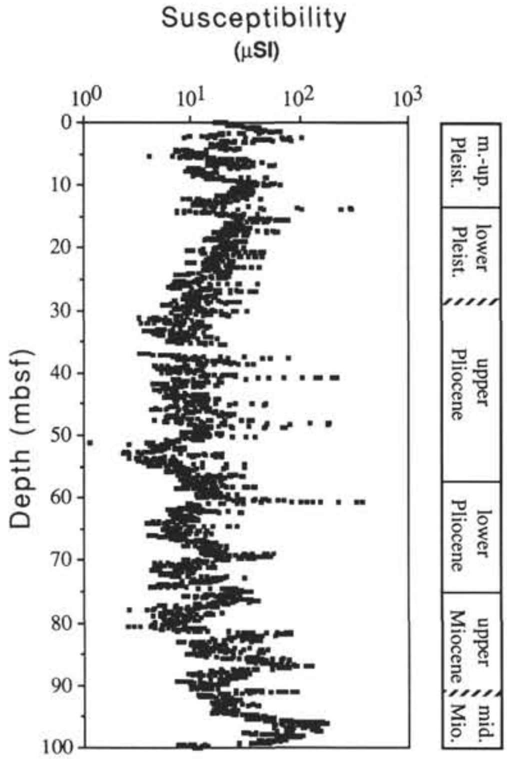

Figure 2. Whole-core magnetic susceptibility variation vs. depth, Hole 810C. Column at right derived from biostratigraphy (Premoli Silva, this volume).

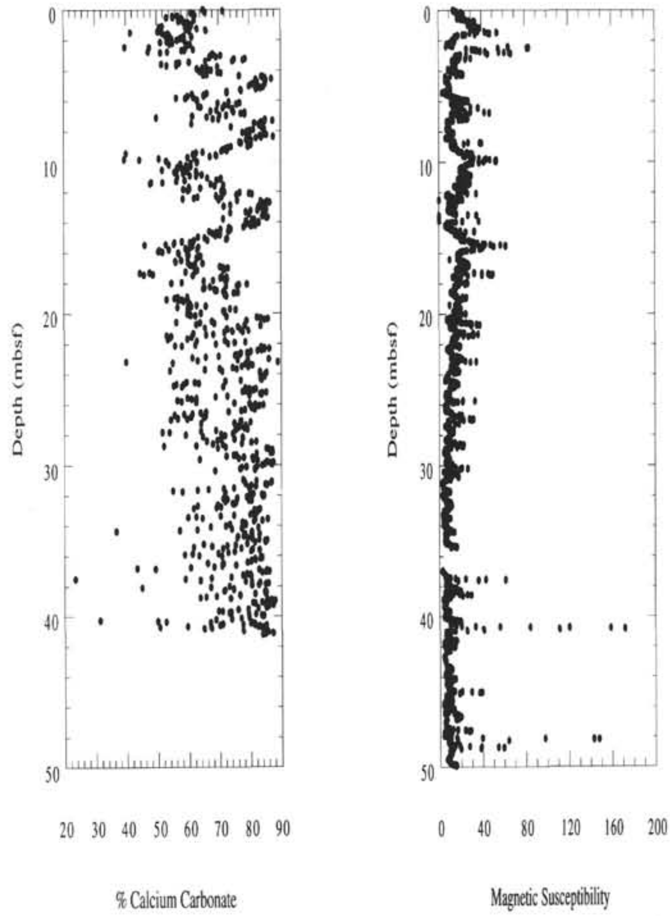

Figure 3. Whole-core magnetic susceptibility and calcium carbonate (after Rack and Janacek, this volume).

lations of about 2 to 3 × 10^{-5} SI, with wavelengths of 5 to 15 m. Slightly smaller fluctuations with peaks on the order of 3 to 5 × 10^{-5} SI and wavelengths of less than 1 m occur between 5 and 8 mbsf and 8 and 12 mbsf and continue downcore. Four spikes greater than 12 × 10^{-5} SI occur: two coincide with ash beds (13.8 and 40.5 mbsf), and two do not (48.2 and 60.6 mbsf). Ash beds do not always appear as large spikes in the magnetic susceptibility record. Of the 21 ash beds, 11 have susceptibility values less than 4 × 10^{-5} SI.

In general, peaks in magnetic susceptibility coincide with the troughs in the calcium carbonate records (Fig. 3). The signal with the 1-m wavelength correlates peak to trough throughout the majority of the record. The same is true of the signal with the 3- to 5-m wavelength. Occasionally, calcium carbonate and magnetic susceptibility records correlate directly rather than inversely. A downward excursion in both records at just below 5 mbsf shows an example of this.

Discrete measurements for the 121 samples from Cores 132-810C-2H and -3H show the same general trends as the whole-core measurements (Fig. 4), and the signal with the 1-m wavelength can be seen more distinctly.

Magnetic Properties

IRM acquisition curves are similar for the majority of the pilot samples. Saturation occurs between 30 and 40 mT, with a fairly sharp bend on approach to saturation, as is typical with magnetite curves (Fig. 5). Most samples, however, also show a slight reluctance to saturate, indicating that they contain high-coercivity magnetic minerals—for example, hematite (Butler, 1982). In contrast, a few samples display a more gradual approach to saturation, implying a greater proportion of high-coercivity minerals than found in more typical samples (Fig. 5). Because these few samples tend to occur preferentially in the tops of Cores 132-810C-2H and -3H, the higher coercivity component may actually be rust introduced into sediments disturbed during the coring process. The uppermost parts of these cores were watery and disturbed by drilling (Storms, Natland, et al., 1991); therefore, it is possible that rust from the drill pipe could have been introduced and mixed into the sediment during coring (Sager, 1986).

A histogram of remanence coercivities shows that the majority of samples are dominated by low-coercivity magnetic minerals (Fig. 6). The remanence coercivities of most samples are in the range 20 to 25 mT. Coercivities of five samples fall between 15 and 20 mT. One sample is between 30 to 35 mT. These values are consistent with laboratory predictions for single-domain magnetite particles. For instance, values for single-domain, equidimensional magnetite particles fall in the range 10 to 15 mT, whereas 30 to 40 mT is typical of single-domain acicular particles. Multidomain particles, on the other hand, have coercivities less than 10 mT (Dunlop, 1986). Of the three samples that give high coercivities of remanence, Sample 132-810C-2H-3, 5–7 cm, gave an anomalous SIRM acquisition curve. This may indicate that the highest coercivities are atypical, perhaps owing to the introduction of some other magnetic mineral into the sediments.

IRM acquisition and demagnetization curves for both high (greater than 10 × 10^{-5} SI) and low (less than 5 × 10^{-5} SI) magnetic susceptibility samples appear strikingly similar, intersecting at essentially the same point (Fig. 7). This could indicate that the dominant magnetic minerals are the same in both high- and low-magnetic susceptibility samples. Except for the anomalous sample, 132-810C-2H-3, 5–7 cm (Fig. 8A), the same is true for ARM and SIRM demagnetization curves (Fig. 8B). For example, most samples, both high- and low-magnetic susceptibility, have ARM demagnetization curves above their SIRM demagnetization curves at low AF demagnetization steps.

In a bilogarithmic scatter plot of SIRM vs. susceptibility, a plot that has been used to describe apparent magnetic grain size (Thompson and

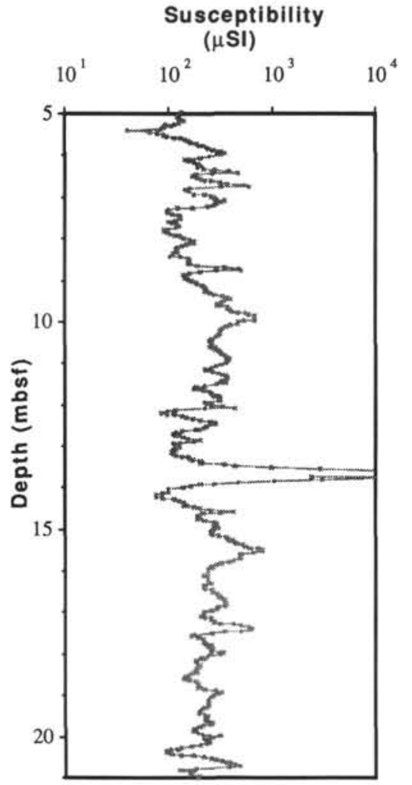

Figure 4. Discrete sample magnetic susceptibility variation vs. depth in the studied parts of Cores 132-810C-2H and -3H.

Oldfield, 1986), samples tend to fall into two apparent size groups, 1 to 2 μm and 2 to 4 μm (Fig. 9). The linearity of each group suggests that the magnetic particle size stays nearly constant, whereas concentration changes tenfold, ranging from about 0.001% to 0.01%. The concentrations and size ranges of Figure 9 only serve as approximate indicators, because this type of diagram was developed from studies of samples containing pure magnetite (Thompson and Oldfield, 1986).

Magnetic-Property Variations vs. Depth

Plots of susceptibility and SIRM with depth correlate strongly (Fig. 10). In fact, within the detailed study section, SIRM/susceptibility is almost constant with depth below 9 mbsf. Because magnetic susceptibility varies primarily with magnetite concentration (Mullins, 1977), this ratio removes much of the concentration effect, so the consistency between SIRM and susceptibility suggests a fairly uniform grain size in this interval. Values between 5 and 9 mbsf are less constant but seem to separate into three linear groups, from roughly 5 to 6 mbsf, 6 to 7 mbsf, and 7.5 to 9 mbsf, which might represent three grain-size or grain-type classes.

Plots of SIRM and ARM with depth correlate relatively well with each other (Fig. 11), again indicating that grain size and/or concentration is fairly consistent. Many of the peaks disappear when SIRM/ARM is plotted with depth, suggesting that these higher frequency fluctuations are mostly concentration effects. However, broader trends remain, perhaps implying subtle shifts in grain size because ARM and SIRM are each sensitive to slightly different grain-size ranges (Maher, 1988). As in the plots of SIRM vs. susceptibility, the area of inconsistency seems to be in the shallower part of the curve, principally between 5 and 7 mbsf. Peaks in SIRM tend to be larger than those in ARM, perhaps owing to a greater concentration of coarser grains (Thompson and Oldfield, 1986).

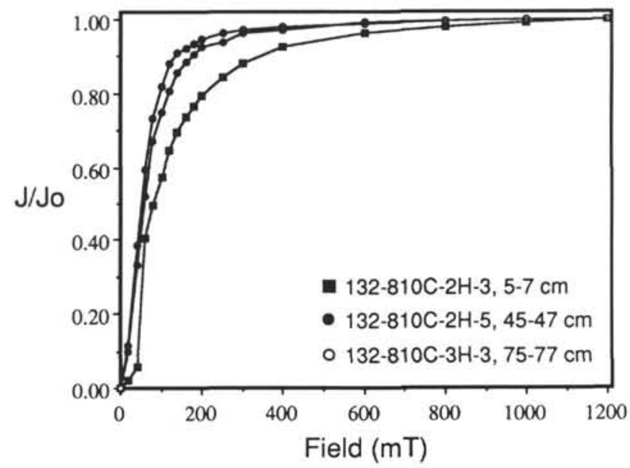

Figure 5. IRM acquisition curves for representative Pleistocene ooze samples, Hole 810C. Samples 132-810C-2H-5, 45–47 cm, and 132-810C-3H-3, 75–77 cm, are from low- and high-susceptibility sediments, respectively. Sample 132-810C-2H-3, 5–7 cm, displays an atypical, high-coercivity signature.

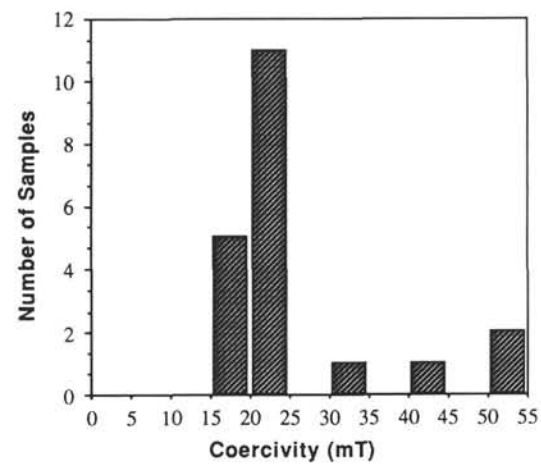

Figure 6. Histogram of remanence coercivities for pilot samples, Hole 810C.

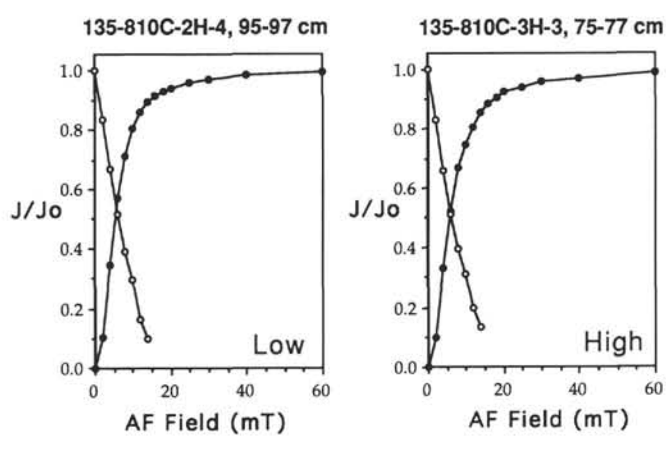

Figure 7. Comparison of IRM acquisition (solid circles) and IRM loss with alternating-field demagnetization (open circles) for high- and low-susceptibility Pleistocene ooze samples.

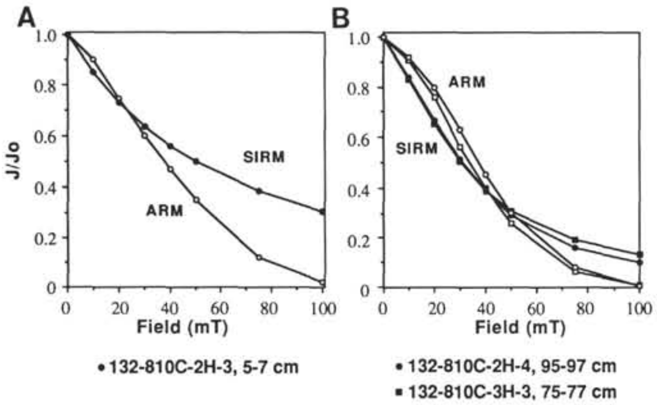

Figure 8. IRM and ARM demagnetization curves for an atypical sample (**A**) and typical high- and low-susceptibility samples (**B**). (See Figure 4.)

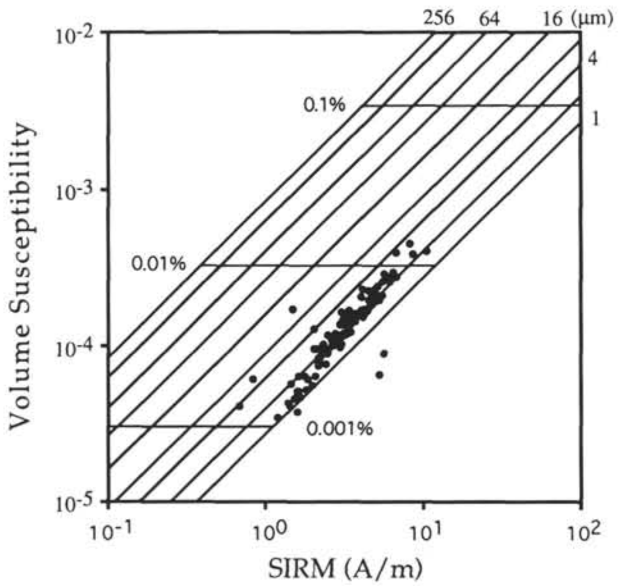

Figure 9. Ratio of magnetic susceptibility to SIRM for samples from the detailed study section. Note that both plot axes are logarithmic. Horizontal and diagonal lines are magnetic grain size and concentration lines derived from studies of pure magnetite (Thompson and Oldfield, 1986); horizontal lines denote concentration, whereas diagonal lines show effect of grain sizes, labeled at top of diagram.

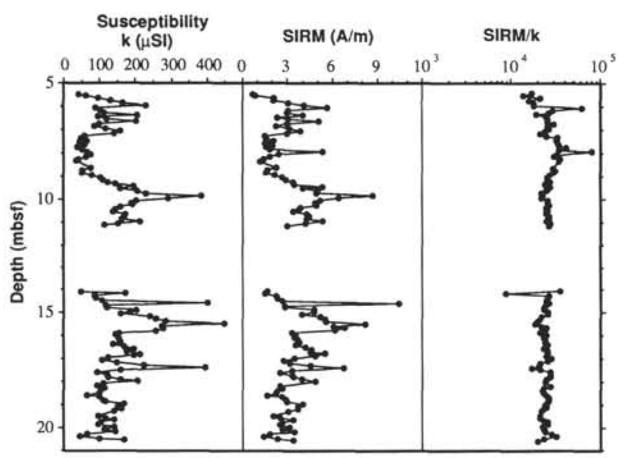

Figure 10. Magnetic susceptibility, SIRM, and SIRM-susceptibility ratios plotted vs. depth for the detailed study section from Hole 810C.

MDF values range from 20 to 60 mT, but most values are within a narrow range, 30 to 40 mT (Fig. 12). Most fluctuation occurs from 5 to 9 mbsf and between 18 and 20 mbsf. These results imply that the magnetic carrier remains relatively constant between 9 and 18 mbsf. Excursions of higher and lower values could result from differences in magnetic-mineral composition or grain size.

Electron Microscopy

The scanning electron microscopy study revealed that high-, medium-, and low-susceptibility samples contain two general size ranges of titanomagnetite grains. The smaller range is approximately 2 to 4 μm, and the larger particles are usually between 10 and 20 μm; a few are even larger, however: one grain measured 75 μm along its long axis, and another was 100 × 50 μm. The discrepancy in size between SIRM-susceptibility ratio indications and SEM observations of larger grains may result from (1) cracking in the larger grains and/or (2) exsolution, which could result in a smaller domain structure.

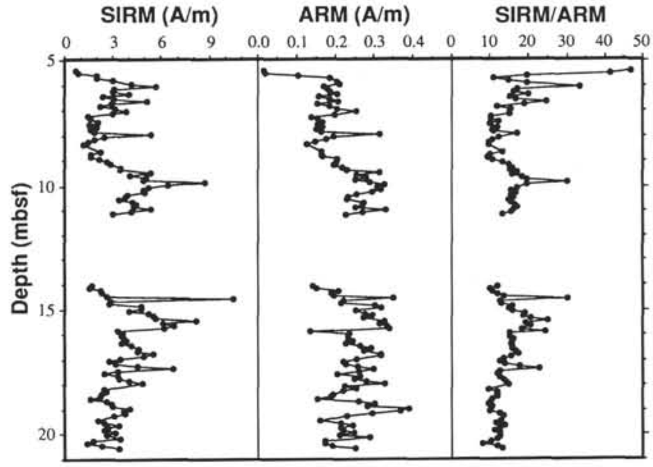

Figure 11. SIRM, ARM, and the ratio of SIRM to ARM plotted vs. depth for the detailed study section.

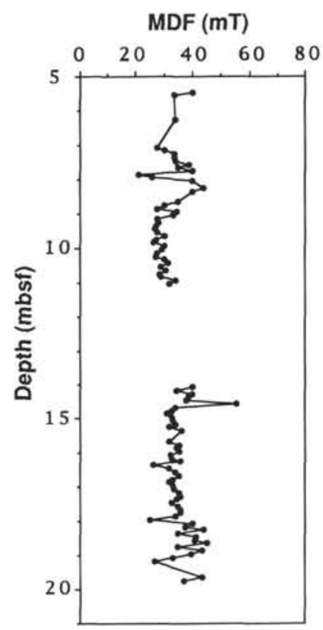

Figure 12. MDF plotted vs. depth for the detailed study section.

Many grains show surface cracking (Fig. 13A). It is difficult to determine whether these cracks invade the interiors of the grains, but if they do, the grains could break into smaller units and hence affect the magnetic-property measurements. Exsolution lattice structures are common in the titanomagnetite grains in these samples. The exsolution process could change the domain structure of the larger grains, causing them to behave as if they were small single-domain grains. Etched magnetite grains (Fig. 13B) suggest a chemically unstable environment for magnetite and argue against the possibility of authigenic formation of euhedral titanomagnetite crystals (Fig. 13C, D) found within the same sample. The magnetic grains vary greatly in shape; some are equidimensional, and others are present as long, thin flat plates. This is consistent with the coercivity data, which contain values typical of both equidimensional and acicular particles.

X-ray-dispersive analysis (EDX) of these three samples usually show the smaller grains to contain more titanium (i.e., Fe:Ti is approximately 4:1) than the larger grains (i.e., Fe:Ti is approximately 17:1). Although no conclusion can be drawn with such a small number of samples examined, the relationship between titanium content and grain size in these samples may suggest the possibility of a different source for each of the two grain-size ranges. An alternative hypothesis could be differential resistance to reduction diagenesis (Bloemendal et al., 1993).

Correlation of Hole 810C with Hole 577

Out of the 117 clear magnetic susceptibility peaks in the data from Hole 810C, only approximately 35% could be correlated with similar features in Hole 577. The match between the two holes is excellent in the top of the Brunhes section (Fig. 14). Patterns A, B, and C show similar shapes and clearly correlate from Hole 810C to Hole 577. Sedimentation rates seem to have remained similar but begin to diverge with pattern C (this multipeak pattern is broader in Hole 810C than its counterpart in Hole 577). Sager et al. (this volume) speculated that changing sedimentation rates could have lengthened the stratigraphic record of the Brunhes at Site 810. The magnetic susceptibility correlation also suggests faster sedimentation at Site 810 during the early Brunhes. Below feature C, the correlation becomes less clear. Pattern D may or may not represent a matched feature, and, clearly, many patterns from Hole 810C are missing from Hole 577 from feature D to the Brunhes/Matuyama Chron boundary (0.73 Ma), including a large spike from one of the Site 810 ash beds (Natland, this volume).

It is difficult to find a match between the two magnetic susceptibility records from the Brunhes/Matuyama Chron boundary to the bottom of the Olduvai Chron (0.73 to 1.88 Ma), but Sager et al. (this volume) note that part of the Matuyama Chron is probably missing at Site 810. From the bottom of the Olduvai Chron to the Matuyama/Gauss Chron

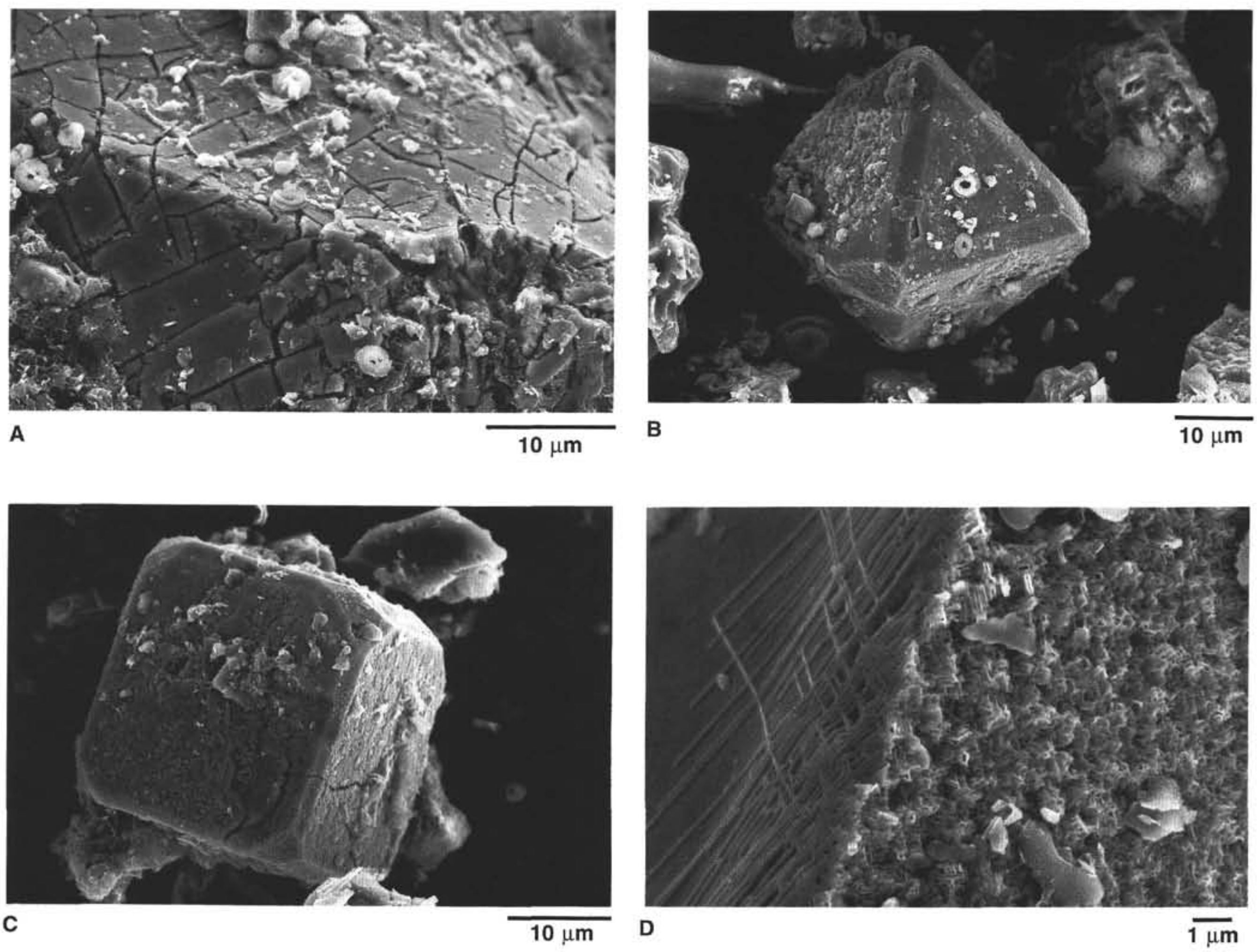

Figure 13. Scanning electron micrographs from Sample 132-810C-2H-3, 86–88 cm. Scale bar = 10 μm for A through C; scale bar = 1 μm for D. **A.** Titanomagnetite grain showing pervasive cracking. **B.** Euhedral titanomagnetite grain. **C.** Euhedral titanomagnetite grain. **D.** Surface of a titanomagnetite grain, showing pervasive pitting on one surface (right) and trellis exsolution pattern on adjacent side (left).

boundary (1.88 to 2.47 Ma), patterns F and G correlate between sites, although sedimentation rates appear higher at Site 810. From the Matuyama/Gauss Chron boundary to the top of the Kaena Chron (2.47 to 2.92 Ma), features H, I, and J also correlate well. Of these, peak I is clearly an ash-bed spike. There is no discernible correlation between the two sites from the top of the Kaena Chron to the bottom of the Mammoth Chron (2.92 to 3.18 Ma). From the bottom of the Mammoth Chron to the Gauss/Gilbert Chron boundary (3.18 to 3.40 Ma) identifiable features K and L occur. Feature M seems to indicate a match just below the Gauss/Gilbert Chron boundary, but a large part of the Site 577 record appears to be missing, resulting both from a gap in the data from just below 43 to about 44.9 mbsf and a depositional hiatus. The top and bottom boundaries of the Cochiti Subchron (3.88 and 3.97 Ma) both seem to be missing in this hole (Bleil, 1985). From this point downward, past the bottom of the Thvera Subchron, no convincing correlation was possible. Feature N may correlate, but if it does, it throws the placement of the top of the Thvera Subchron into question because it crosses the boundary. From the bottom of the Thvera Subchron to the base of the Gilbert Chron (4.77 to 5.35 Ma), pattern O clearly matches from site to site. Below this, P and Q also match from record to record.

DISCUSSION

Magnetic Minerals

This study suggests that first-order susceptibility cycles are caused by variations in the concentration of the primary magnetic carrier rather than changes in mineralogy or grain size. Magnetic properties show little variation and, in general, do not correlate with susceptibility peaks. IRM acquisition and demagnetization plots and ARM demagnetization curves appear identical for both high- and low-susceptibility samples.

Indicators of grain size also seem largely independent of these first-order susceptibility cycles. The SIRM vs. susceptibility ratio suggests a general size range of 1–4 μm with two groupings of data points. The samples within these groups track the larger scale, broad systematic decrease and increase of 50×10^{-6} SI that takes place between the lower Pleistocene and the middle Miocene. Plots of SIRM/susceptibility and SIRM/ARM with depth also suggest a fairly constant grain size, with the latter suggesting a bias toward larger grains. Remanence coercivities also suggest the presence of pseudo-single-domain grains. Our electron microscopy study shed further light on the grain sizes of magnetic minerals within high-, medium-, and low-susceptibility samples. Two size ranges were identified, which are independent of the size groupings described by the SIRM/susceptibility plot, since they are found in all the samples examined. These ranges are approximately 2–4 μm and 10–20 μm, the latter being larger than sizes predicted by the SIRM/susceptibility plot, but this discrepancy between theoretically predicted and observed grain size could be explained by the breakdown of the grains by cracking and exsolution. The smaller, titanium-rich magnetite particles observed in the SEM may have been derived from an influx of ash and the lower titanium, and larger particles could represent other terrestrial sediment. Two sources, the Chinese plateau and the Japanese arc, have been suggested for the magnetic minerals of nearby Site 577 (Doh, 1987). The existence of smaller Ti-rich grains may also result from differential reduction diagenesis in which those grains that contain smaller amounts of titanium are preferentially dissolved (Bloemendal et al., 1993).

We conclude that these first-order susceptibility fluctuations are largely independent of both mineralogy and grain size and, therefore, must result from a concentration effect in which the input or dilution of magnetic minerals varies, or both.

Correlation of Hole 810C with Hole 577

To characterize the sedimentation of Site 810 and to test the potential of its magnetic susceptibility record for regional correlation, we compared this record to the magnetic susceptibility record of Site 577. Because the distance between the sites is small and both sites are located at roughly the same water depth, we expected the sites to correlate closely. Of the 117 easily identifiable peaks in the record of Hole 810C, only 41 (35%) match peaks in Site 577. This lack of correlation between two sites only 11.7 km apart and differing only 50 m in bathymetric depth is curious. It probably results from differing depositional rates and erosion at the two sites. Sedimentary features in one record typically seem to be missing in the other. For instance, there were 22 pumice and ash beds noted at Hole 810C but only 3 at Hole 577 (Heath, Burkle, et al., 1985; Natland, this volume). Comparison of magnetic stratigraphy between the two sites also implies differing average sedimentation rates (Sager et al., this volume). Moreover, missing magnetochrons as well as differing magnetochron thicknesses between Holes 577 and 577A (Bleil, 1985), only a few tens of meters apart, argue for significant differences in sedimentation over very short distances. Sager et al. (this volume) suggested that currents atop these topographic highs could account for inconsistent deposition between these two sites. Varying smear-slide textures may also provide evidence for erosion and reworking. Sand-sized grains are usually present in negligible amounts, but they represent as much as 70%–100% of the texture in a few places (Storms, Natland, et al., 1991; Heath, Burkle, et al., 1985). One could argue that poor correlation between the two sites results from recovery having been less complete in the cores from Hole 577. The recovery for the piston-cored sediments in Hole 810C ranges from 100% to 105.9% (Storms, Natland, et al., 1991). Percentages over 100 are probably caused by expansion of the sediments within the core liner. Recovery for Hole 577 falls between 84% and 101% (Heath, Burkle, et al., 1985). Given this difference, we might expect that roughly 8% of the features to be missing in the record from Hole 577, so relatively poorer recovery at Site 577 cannot explain why only 35% of the features match between the two sites. The fact that correlation is poor over such a small geographical distance, coupled with the lack of constancy of deposition, means that only parts of the record may be suitable for use in time- and frequency-domain paleoclimate studies.

SUMMARY AND CONCLUSIONS

Both whole-core and discrete susceptibility measurements show two levels of variation: larger scale trends that vary over spans of tens of meters and smaller wavelength fluctuations of 1 m or less.

Ash beds do not always appear as large spikes in the magnetic susceptibility record. Overall, magnetic susceptibility values are predominantly negatively correlated with calcium carbonate percentages. Similar variations in other deep-sea sediments have been interpreted as records of glacial-interglacial climate cycles.

From our study of the magnetic properties, we reached the following conclusions: (1) the magnetic properties of the Hole 810C cores are dominated by titanomagnetite but also contain a variable fraction of higher coercivity minerals such as hematite or goethite; (2) the titanomagnetite grains show a restricted size range and possibly single-domain or pseudo-single-domain behavior; (3) high- and low-susceptibility samples have similar magnetic properties; (4) the high-frequency magnetic susceptibility fluctuations, identified as possible glacial/interglacial signals, seem to be largely independent of grain size and mineralogy; and (5) these magnetic susceptibility fluctuations must result from a concentration effect in which input varies, dilution varies, or both. The magnetic properties indicate that these records could be used in paleoclimate studies.

Scanning electron microscopy and energy-dispersive X-ray analyses show titanomagnetite with dissolution features in some of the grains. Energy-dispersive X-ray analysis of a few samples suggests two basic size fractions with different titanium concentrations. These observations suggest magnetic grains transported from two source regions or differential reduction diagenesis of the titanomagnetite grains.

In our study of the correlation between Sites 810 and 577, we found that, in all, only 35% of the peaks match from site to site. This

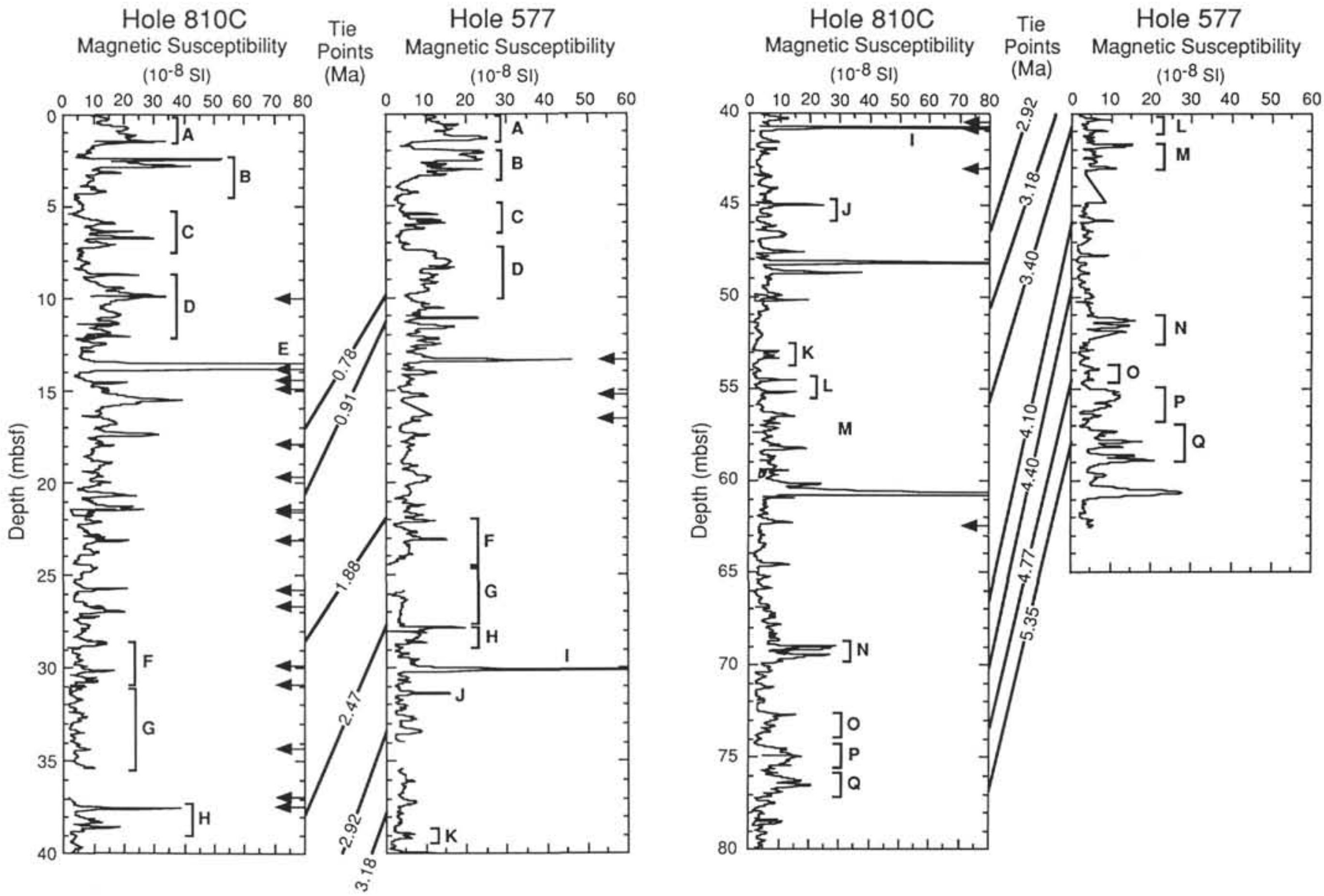

Figure 14. Correlation of whole-core susceptibility measurements between Hole 810C and Hole 577. Letters denote characteristic peaks or patterns of peaks that can be correlated between holes. Labeled diagonal lines are correlation points from magnetostratigraphic polarity boundaries (Bleil, 1985; Sager et al., this volume) and give ages in millions of years. Arrows represent ash layers.

paucity of correlatable features suggests that sedimentation atop Shatsky Rise has been uneven or disturbed by local erosion. Missing features at Site 577 suggest a greater degree of erosion and perhaps stronger currents at that site. As a consequence of possible erosion at both sites, it may be difficult to obtain continuous sediment sections with adequate time control for paleoclimate studies in this locality.

ACKNOWLEDGMENTS

We thank JOI/USSAC for providing financial support. We acknowledge Jack Baldauf, John King, and Laura Stokking for their helpful reviews. We thank Tom Janecek for providing calcium carbonate data for Hole 810C.

REFERENCES*

Berggren, W.A., Kent, D.V., Flynn, J.J., and Van Couvering, J.A., 1985. Cenozoic geochronology. *Geol. Soc. Am. Bull.,* 96:1407–1418.

Bleil, U., 1985. The magnetostratigraphy of northwest Pacific sediments, Deep Sea Drilling Project Leg 86. *In* Heath, G.R., Burckle, L.H., et al., *Init. Repts. DSDP,* 86: Washington (U.S. Govt. Printing Office), 441–458.

* Abbreviations for names of organizations and publications in ODP reference lists follow the style given in *Chemical Abstracts Service Source Index* (published by American Chemical Society).

Bloemendal, J., and deMenocal, P., 1989. Evidence for a change in the periodicity of tropical climate cycles at 2.4 Myr from whole-core magnetic susceptibility measurements. *Nature,* 342:897–900.

Bloemendal, J., King, J.W., Hall, F.R., and Doh, S.-J., 1992. Rock magnetism of late Neogene and Pleistocene deep-sea sediments: relationship to sediment source, diagenetic process, and sediment lithology. *J. Geophys. Res.,* 97:4361–4375.

Bloemendal, J., King, J.W., Hunt, A., deMenocal, P.B., Hayashida, A., 1993. Origin of the sedimentary magnetic record at Ocean Drilling Program sites on the Owen Ridge, western Arabian Sea. *J. Geophys. Res.,* 98:4199–4219.

Bloemendal, J., Lamb, B., and King, J., 1988. Paleoenvironmental implications of rock-magnetic properties of late Quaternary sediment cores from the eastern equatorial Atlantic. *Paleoceanography,* 3:61–87.

Butler, R.F., 1982. Magnetic mineralogy of continental deposits, San Juan Basin, New Mexico and Clark's Fork Basin, Wyoming. *J. Geophys. Res.,* 87B:7843–7852.

Cande, S.C., and Kent, D.V., 1992. A new geomagnetic polarity timescale for the Late Cretaceous and Cenozoic. *J. Geophys. Res.,* 97:13917–13951.

Doh, S.-J., 1987. Magnetic studies of marine sediments [Ph.D. thesis]. Univ. of Rhode Island, Narragansett.

Dunlop, D.J., 1986. Hysteresis properties of magnetite and their dependence on particle size: a test of pseudo-single-domain remanence models. *J. Geophys. Res.,* 91:9569–9584.

Heath, G.R., Burckle, L.H., et al., 1985. *Init. Repts. DSDP,* 86: Washington (U.S. Govt. Printing Office).

Hovan, S.A., Rea, D.K., Pisias, N.G., and Shackleton, N.J., 1989. A direct link between the China loess and marine $\delta^{18}O$ records: aeolian flux to the North Pacific. *Nature,* 340:296–298.

Kent, D.V., 1982. Apparent correlation of paleomagnetic intensity and climatic records in deep-sea sediments. *Nature,* 299:538–539.

Kukla, G., and An, Z., 1989. Loess stratigraphy in central China. *Palaeogeogr., Palaeoclimatol., Palaeoecol.,* 72:203–225.

Kukla, G., Heller, F., Ming, L.X., Chun, X.T., Sheng, L.T., and Sheng, A.Z., 1988. Pleistocene climates in China dated by magnetic susceptibility. *Geology,* 16:811–814.

Maher, B.A., 1988. Magnetic properties of some synthetic sub-micron magnetites. *Geophys. J.,* 94:83–96.

Maher, B.A., and Thompson R., 1992. Paleoclimatic significance of the mineral magnetic record of the Chinese loess and paleosols. *Quat. Res.,* 37:155–170.

Mead, G.A., Tauxe, L., and LaBrecque, J.L., 1986. Oligocene paleoceanography of the South Atlantic: paleoclimatic implications of sediment accumulation rates and magnetic susceptibility. *Paleoceanography,* 1:273–284.

Mullins, C.E., 1977. Magnetic susceptibility of the soil and its significance in soil science–a review. *J. Soil Sci.,* 28:223–246.

Rea, D.K., and Leinen, M., 1988. Asian aridity and the zonal westerlies: late Pleistocene and Holocene record of eolian deposition in the Northwest Pacific Ocean. *Palaeogeogr., Palaeoclimatol., Palaeoecol.,* 66:1–8.

Robinson, S.G., 1986. The late Pleistocene paleoclimatic record of North Atlantic deep-sea sediments revealed by mineral-magnetic measurements. *Phys. Earth Planet. Inter.,* 42:22–47.

Sager, W.W., 1986. Magnetic-susceptibility measurements of metal contaminants in ODP Leg 101 cores. *In* Austin, J.A., Jr., Schlager, W., et al., *Proc. ODP, Init. Repts.,* 101: College Station, TX (Ocean Drilling Program), 39–46.

Storms, M.A., Natland, J.H., et al., 1991. *Proc. ODP, Init. Repts.,* 132: College Station, TX (Ocean Drilling Program).

Thompson, R., and Oldfield, F., 1986. *Environmental Magnetism:* London (Allen and Unwin).

Date of initial receipt: 10 December 1992
Date of acceptance: 29 June 1993
Ms 132SR-303